12180 *Biochemistry* **2009,** *48,* 12180–12190
DOI: 10.1021/bi9017076

BIOCHEMISTRY
including biophysical chemistry & molecular biology
Article

The $\beta\gamma$-Crystallin Superfamily Contains a Universal Motif for Binding Calcium[†,‡]

Penmatsa Aravind,[§] Amita Mishra,[§] Shashi Kumar Suman,[§] Maroor K. Jobby,[∥] Rajan Sankaranarayanan,* and Yogendra Sharma*

Centre for Cellular and Molecular Biology, Council of Scientific and Industrial Research, Uppal Road, Hyderabad 500007, India. [§]*These authors contributed equally.* [∥]*Present address: Department of Biochemistry, Queen's University, Kingston, Ontario, Canada K7L 3N6.*

Received October 2, 2009; Revised Manuscript Received November 17, 2009

ABSTRACT: The $\beta\gamma$-crystallin superfamily consists of evolutionarily related proteins with domain topology similar to lens β- and γ-crystallins, formed from duplicated Greek key motifs. Ca^{2+} binding was found in a few $\beta\gamma$-crystallin members earlier, although its prevalence and diversity as inherent molecular properties among members of the superfamily are not well studied. To increase our understanding of Ca^{2+} binding in various $\beta\gamma$-crystallins, we undertook comprehensive structural and Ca^{2+}-binding studies of seven members of the superfamily from bacteria, archaea, and vertebrates, including determination of high-resolution crystal structures of three proteins. Our structural observations show that the determinants of Ca^{2+} coordination remain conserved in the form of an N/D-N/D-#-I-S/T-S motif in all domains. However, binding of Ca^{2+} elicits varied physicochemical responses, ranging from passive sequestration to active stabilization. The motif in this superfamily is modified in some members like lens crystallins where Ca^{2+}-binding abilities are partly or completely compromised. We show that reduction or loss of Ca^{2+} binding in members of the superfamily, particularly in vertebrates, is due to the selective presence of unfavorable amino acids (largely Arg) at key Ca^{2+}-ligation positions and that engineering of the canonical Ca^{2+}-binding residues can confer binding activity on an otherwise inactive domain. Through this work, we demonstrate that $\beta\gamma$-crystallins with the N/D-N/D-#-I-S/T-S motif form an extensive set of Ca^{2+}-binding proteins prevalent in all of the three kingdoms of life.

Ca^{2+} binding is a crucial step in affecting major life processes (*1*) with specialized protein motifs engineered by nature to bind Ca^{2+} with varied affinities in both the extracellular and intracellular environments (*2*). Proteins evolved to sense Ca^{2+} as a signal are commonly referred to as sensors, and a set of proteins that bind and undergo structural stabilization are referred to as buffers. The all α-helical EF-hand superfamily of proteins and all β-sheet containing C2 domains predominate sensory Ca^{2+}-binding proteins. Proteins involved in structural binding are found in many extracellular proteins, such as EGF domains and cadherins, and are involved in providing structural stability to an organism by sequestering Ca^{2+} from the environment. All of these independent structural units have been recruited as full-length proteins or as modules in multidomain proteins to perform Ca^{2+}-dependent roles.

Apart from these known families of Ca^{2+}-binding proteins, some members of $\beta\gamma$-crystallins have been shown to bind Ca^{2+}. The $\beta\gamma$-crystallin superfamily comprises proteins with β-sandwich domains whose early characterized members, β- and γ-crystallins, are major components of the vertebrate eye lens (*3*−*5*). Individual $\beta\gamma$-crystallin domains are made of strand-exchanged Greek key motifs (*6*, *7*). The wedge-like domains are characterized by the presence of highly ordered β-hairpin loops between the first and second strands of each motif. Two loops traverse the roof of the wedge-like domain and connect the two opposing β-pleated sheets of the domain (*6*−*8*). Evolutionarily related structural homologues of lens β- and γ-crystallins are found in some lower eukaryotic and prokaryotic species which together form the $\beta\gamma$-crystallin superfamily.

The Ca^{2+}-binding connection to the $\beta\gamma$-crystallin superfamily was observed more than 2 decades ago when protein S from *Myxococcus xanthus*, the first member of the superfamily, was shown to bind Ca^{2+} even before the classification of the $\beta\gamma$-crystallin superfamily (*7*, *9*, *10*). At the same time, β-crystallin (aggregated form) from the vertebrate lens was shown to bind Ca^{2+} albeit with low affinity in solution and with no structural evidence for the Ca^{2+}-binding site (*11*). When the sequence of spherulin 3a from *Physarum polycephalum* was described with the putative features of $\beta\gamma$-crystallins as a third member, the concept of a superfamily, the $\beta\gamma$-crystallin superfamily originated (*12*). Spherulin 3a was structurally characterized and found to have bound Ca^{2+} at the D/N-X-X-S motif, similar to that seen first in protein S (*13*−*15*). Later, a few members of this superfamily were demonstrated to bind Ca^{2+} in solution (*16*−*19*). Protein S and spherulin 3a remained the only structurally well characterized Ca^{2+}-binding members of the $\beta\gamma$-crystallin superfamily

[†]This work was supported by a Department of Science and Technology and a DBT grant to Y.S. and a Swarnajayanti Fellowship, DST, India, and an International Senior Research Fellowship, Wellcome Trust, U.K., grant to R.S. P.A. and S.K.S. are the recipients of fellowships from the Council of Scientific and Industrial Research, India. A. M. is supported by a postdoctoral fellowship from the Department of Biotechnology, India.

[‡]The coordinates and structure factor amplitudes of M-crystallin, clostrillin (forms 1 and 2), and flavollin have been deposited in the Protein Data Bank with the IDs 3HZ2, 3I9H, 3IAJ, and 3HZB, respectively.

*Corresponding authors. Y.S.: phone, +91-40-27192544; fax, +91-40-27160591; e-mail, yogendra@ccmb.res.in). R.S.: phone, +91-40-27192832; fax, +91-40-27160591; e-mail, sankar@ccmb.res.in.

 Published on Web 11/18/2009

(*8*, *13*−*15*, *20*, *21*) until the structure of *Ciona* crystallin, an ancestral family member from urochordates that do not have a lens, was solved in Ca^{2+}-bound form, shedding light on the evolution of lens $\beta\gamma$-crystallins (*22*). Incidentally, the Ca^{2+}-binding region in these three proteins was located at the homologous D/N-X-X-S motif.

These sporadic studies opened up several interesting questions to be explored, particularly about the detailed description of Ca^{2+} binding as well as the motif of ion binding. This is necessary since Ca^{2+}-binding motifs are well-defined supersecondary structures, as in the case of the EF-hand motif. Earlier studies were largely focused on the evolutionary aspects of crystallins, in addition to Ca^{2+} binding. Therefore, first of all, an important question to address is whether the sequence D/N-X-X-S forms a specific, well-defined motif for Ca^{2+} binding prevalent in other proteins of the superfamily or presents only in a few $\beta\gamma$-crystallins as a unique case. One of the reasons was that a large number of proteins have not been shown to bind Ca^{2+} ions (in some cases even structurally), such as yeast killer toxins, SKLP,[1] SMPI, AIM1g1, and nitrollin (*23*−*27*). In addition to this, not many members belonging to the $\beta\gamma$-crystallin superfamily were known until recently. On the other hand, several proteins, such as *Yersinia* crystallin (*16*), caulollins (*17*), AIM1 domain (*28*), and geodin (*19*), have been shown to bind Ca^{2+} only in solution but without any structural evidence for a homologous Ca^{2+}-binding motif.

With these ambiguities, it became necessary to clarify several questions: (i) Does the sequence D/N-X-X-S seen in spherulin 3a and protein S form a widespread motif of Ca^{2+} binding in the superfamily? (ii) What would be the effects of sequence diversification of motif on the Ca^{2+}-binding properties of individual proteins? (iii) If the motif is well-defined, could a gain of function be created in a naturally disabled protein? In order to understand and explore some of these outstanding questions pertaining to $\beta\gamma$-crystallins and their Ca^{2+}-binding properties, we undertook this extensive structural characterization by identifying proteins belonging to this family from all three kingdoms of life (archaeal, bacterial, and eukaryote including vertebrate species).

Our analysis of the genomes from various species demonstrates the prevalence of the proteins with $\beta\gamma$-crystallin-like domains. This Ca^{2+}-binding motif is widely present in close to 70 independent proteins from various species across all three kingdoms of life. Our in-depth structural analysis of novel proteins, along with earlier observations of Ca^{2+} binding in three $\beta\gamma$-crystallin homologues, suggests that the Ca^{2+}-binding sequence seen earlier actually forms a motif for Ca^{2+} binding. Since we were able to create a gain of Ca^{2+}-binding function in the naturally disabled protein, nitrollin, a domain-swapped $\beta\gamma$-crystallin from *Nitrosospira multiformis* (*27*), we suggest that this ancestral motif was modified and lost Ca^{2+} binding in some descendant lineages. Our data comprehensively confirm the widespread conservation of this motif for Ca^{2+} binding, which has undergone extensive modifications in several descendants, including many vertebrates.

EXPERIMENTAL PROCEDURES

Genomic DNA and Clones from Various Species. The genomic DNA of *Flavobacterium johnsoniae*, *Methanosarcina acetivorans*, *Reinekea* sp. MED297, and *N. multiformis* were kind gifts from Dr. Mark J. McBride, University of Wisconsin, Professor William W. Metcalf, University of Illinois at Urbana−Champaign, Dr. Jarone Pinhassi, University of Kalmar, Sweden, and Dr. Lisa Stein, University of California, Riverside, respectively. The region of interest (500−591 amino acids) of the protein YP_001196503 from *F. johnsoniae* and 36−120 amino acids of a protein annotated as the $\beta\gamma$-crystallin family protein (accession number AAM05909) from *M. acetivorans* were amplified by using gene-specific primers. Genomic DNA of *Clostridium beijerincki* and *Rhodoferax ferrireducens* strains (obtained from DSMZ, Germany) were isolated using the hot phenol method. Similarly, clostrillin ($\beta\gamma$-crystallin domains of 118−180 amino acids) of the protein (accession number YP_001309930) from *C. beijerinckii*, rhodollin (22−117 amino acids) of the protein (accession number YP_522648) from *R. ferrireducens*, reinekillin (356−536 amino acids) of the protein (ZP_01115288) from *Reinekea* sp. D297, and nitrollin (32−140 amino acids) of the protein (accession number YP_411671) from *N. multiformis* were amplified. ep-37A1 (epidermal differentiation-specific protein) (clone BAA21832) from adult *Cynops pyrrhogaster*, an amphibian, was a kind gift from Dr. Kazuhito Takeshima, Nagoya University, Japan.

Cloning and Overexpression of Untagged and Tagged Proteins. PCR products of $\beta\gamma$-crystallin homologues from *F. johnsoniae*, *M. acetivorans*, *C. beijerinckii*, *R. ferrireducens*, and *N. multiformis* were cloned in a pET21a expression vector (Novagen) at *Nde*I and *Bam*HI sites. PCR fragments from *Reinekea* and ep37 were cloned in a pGEX-4T1 (GE Healthcare) vector at *Bam*HI and *Eco*RI sites. The recombinant proteins flavollin, M-crystallin, and nitrollin were expressed in the bacterial strain *Escherichia coli* BL21(DE3) (Invitrogen) in LB medium (containing 100 μg of ampicillin/mL) after induction with 1 mM isopropyl thio-β-D-galactopyranoside (IPTG) for 10 h at 37 °C. The overexpression of clostrillin, reinekillin, rhodollin, and ep37 was performed by growing *E. coli* BL21(DE3) at 18 °C for 16−18 h after induction with 1 mM IPTG.

Protein Purification. Proteins which formed inclusion bodies during overexpression (flavollin, rhodollin, and nitrollin) were refolded using an on-column refolding procedure. The inclusion bodies were washed with 1 M urea and 0.1% CHAPS and were solubilized in a buffer containing 50 mM Tris buffer, pH 8.5, or 50 mM Bis-Tris, pH 6.2, 3.5−5 M urea, and 1 mM DTT, and on-column refolding was performed on Q-Sepharose for flavollin and on SP-Sepharose matrix for nitrollin. The yield of flavollin and nitrollin per liter of culture was 1.8 and 0.8 mg, respectively. Rhodollin was purified using SP-Sepharose matrix in 50 mM sodium acetate, pH 5.0, 5.0 M urea, and 1 mM DTT. The proteins were eluted with a step gradient of 50 mM Tris, pH 8.5, or Bis-Tris, pH 5.5, 1 M NaCl, and 1 mM DTT with a final yield of 0.5 mg/L of culture. Clostrillin was purified from the soluble fraction on a Q-Sepharose column at pH 9.6 (yield per liter of culture was 8.5 mg). GST-tagged proteins (Reinekillin, ep37) were purified on a GST fast-flow column using prescribed protocols (GE healthcare), and the yield was about 2 mg/L of LB culture. Final purification of flavollin, clostrillin, rhodollin, and nitrollin was performed using Superdex-75 gel filtration columns. ep37 and reinekillin were purified on a Superose-12 gel filtration column (Pharmacia). M-crystallin was purified from a soluble fraction through a Bio-Gel A-1.5 m gel filtration column in 50 mM Tris-HCl (pH 7.5) and 100 mM KCl, and the yield was about 2.5 mg/L of culture. Protein concentrations were calculated

[1]Abbreviations: AIM1, absent in melanoma 1; EDTA, ethylenediaminetetraacetic acid; SKLP, *Streptomyces* killer toxin-like protein; SMPI, *Streptomyces* metalloproteinase inhibitor.

by measuring their absorbance at 280 nm in 6 M guanidinium chloride using the values of the theoretical extinction coefficient calculated by the ExPASy Proteomics Server (ProtParam).

Crystallization. The purified proteins were exchanged into a buffer containing 10 mM Tris, pH 7.2, 20 mM NaCl, 3−5 mM $CaCl_2$, and 0.02% sodium azide. A stock solution of 10 mg/mL was used for setting up screens in the 96-well format in Greiner plates by sitting drop vapor diffusion through mixing 1 μL of protein with 1 μL of reservoir solution with concentrations of 5, 8, and 10 mg/mL in each of the subwells, respectively. Two commercial screens, Crystal Screen HT and Index HT (Hampton Research), were used for screening at a temperature of 4 or 20 °C in our in-house HT facility which employs a Minstrel (Rigaku) plate incubator and imaging system. M-crystallin crystallized in the F10 condition of Crystal Screen HT which comprises 12% PEG 20K with 0.1 M Na-MES, pH 6.5 at 20 °C; flavollin crystals were obtained in 30% PEG 8K with 0.1 M sodium cacodylate buffer at pH 6.5 with 0.4 M potassium chloride. Form 1 crystals of clostrillin crystallized in 26% PEG 3350 at pH 7.3 maintained using 0.1 M HEPES buffer with 0.2 M lithium sulfate; form 2 crystals were obtained in 2 M ammonium sulfate at pH 6.5 maintained using 0.1 M Bis-Tris.

Data Collection and Processing. X-ray data were collected in-house using a mar345dtb image-plate detector attached to a Rigaku RU-H3R rotating anode generator equipped with an osmic mirror system operated at 50 kV/100 mA. Data for flavollin crystals were collected at the X11 beamline at DESY, EMBL-Hamburg. All of the data sets were processed and scaled using DENZO and SCALEPACK (*29*). Conversion of reflection formats, merging, and scaling of reflections were performed using the CCP4 suite of programs, version 6.0 (*30*).

Structure Determination. Structures of clostrillin, M-crystallin, and flavollin were solved using molecular replacement using MOLREP and BALBES (*31*). Structures of *Ciona* crystallin (2BV2) and protein S (1NPS) were used as templates to solve the structures. M-crystallin and form 1 and form 2 structures of clostrillin were solved using the automated molecular replacement program MOLREP from the CCP4 package, version 6.0 (*30*). The form 1 structure of clostrillin had two sets of four protomers (eight molecules/AU) related among each other by an approximate 4-fold symmetry. The two sets of molecules were related by a pseudotranslation vector of (0.0, 0.34, 0.5) which resulted in a nonorigin peak in the Patterson map whose intensity was 34% of the origin peak. MOLREP found six molecules in the AU, and the remaining two were positioned by using the pseudotranslation vector. The structure of flavollin was solved in the *P*2 space group although the initial estimates indicated *I*222 in which the structure could be solved but could not be refined. This disparity arose due to pseudomerohedral twinning that occurred as a result of the angle "β" of the monoclinic space group being close to 90°. This led *P*2 to emulate the *P*222 system. A further complication occurred as the crystals had pseudobody centering (Patterson vector 0.5, 0.5, 0.5, nonorigin peak equivalent to 58% of the origin peak) which led to the P222 space group emulating the *I*222 lattice. Initial diagnosis and molecular replacement were performed using BALBES which picked protein S (1NPS) as a probe (*31*). The partially refined structure of flavollin was then used to perform the complete structure solution and refinement. Nitrollin structure solution was performed using multiple isomorphous replacement as described earlier (*27*).

Refinement and Structural Analysis. Model building in required regions of the structure was performed using the program "O" (*32*) with repeated cycles of refinement using the CNS program package (*33*). All of the refined structures were validated using PROCHECK (*34*) (Table 1). Distance measurements were performed both manually in O and using EBI-PISA (*35*). Structural deviations were calculated using the DALILITE server (*36*).

Isothermal Calorimetric Titration. All of the Ca^{2+}-binding experiments were carried out in a Microcal VP-ITC instrument. Protein samples and calcium chloride (10 mM) were prepared in a Chelex-treated 50 mM Tris, pH 7.0, and 100 mM KCl buffer. A total of 1.6 mL of protein solution in the concentration range of 70−100 μM was used for binding at 30 °C using $CaCl_2$ as ligand solution with 2 μL of injection volume for each titration. Blanks were obtained by titrating the buffer with the same concentration of Ca^{2+}. Curve fitting was performed using the software Origin (version 7) supplied by MICROCAL.

Fluorescence and Circular Dichroism Spectroscopy. Fluorescence emission spectra were recorded on a F-4500 Hitachi fluorescence spectrophotometer with proteins in 0.1 mg/mL concentration. Trp fluorescence was recorded between 300 to 400 nm using an excitation wavelength of 295 nm in 50 mM Tris-HCl, pH 7.0, and 100 mM KCl. Thermal unfolding experiments were performed by monitoring the change in ellipticity at 218 nm on a Jasco J-815 spectropolarimeter from 25 to 85 °C in a 1 mm path length cuvette with appropriate protein concentrations in the presence of either EDTA or Ca^{2+}.

Data Deposition. The coordinates and structure factor amplitudes of M-crystallin, clostrillin (forms 1 and 2), and flavollin have been deposited in the Protein Data Bank with the IDs 3HZ2, 3I9H, 3IAJ, and 3HZB, respectively. Crystal structures of nitrollin wild type were deposited earlier under the PDB IDs 3ENU and 3ENT.

RESULTS

Novel Homologues of $\beta\gamma$-Crystallins. Using protein sequences of known $\beta\gamma$-crystallins as templates, we retrieved putative sequences of diverse species from the database using BLAST searches. Protein BLAST was performed using protein sequences containing the $\beta\gamma$-crystallin sequence signature of F/YXXXXF/YXG. All BLAST searches were performed using protein sequences corresponding to one domain length of sequence (~90 residues) and were searched for nonredundant protein sequences across a wide range of organisms and phyla. The retrieved sequences were analyzed manually for the presence of $\beta\gamma$-crystallin-type features. $\beta\gamma$-Crystallin domains are β-sandwich domains with two Greek keys sharing their third strand during domain folding. The sequence signatures lie in the presence of F/YXXXXF/YXG region after the first strand that forms a bent hairpin loop between strands 1 and 2 and subsequently strands 5 and 6 in the domain.

Genomic sequences from multiple species have revealed the presence of $\beta\gamma$-crystallin domains either as independent proteins or in conjunction with domains of different functions (Figure 1). The recruitment happens across all three kingdoms of life with particular prominence in prokaryotes (Figure 1). Since many proteins were annotated as hypothetical proteins, we christened them; a protein from *F. johnsoniae* was named as flavollin (flavobacterium + crystallin). We chose proteins from seven independent species covering archaea, bacteria, and eukarya (vertebrate): M-crystallin from *M. acetivorans* (archaea), clostrillin from *C. beijerinckii* (Gram +ve prokaryote), flavollin from *F. johnsoniae* (Gram −ve prokaryote), rhodollin from

Table 1: Crystallographic Data and Refinement Statistics

	M-crystallin	flavollin	clostrillin form 1	clostrillin form 2
Data Statistics				
source	Cu Kα	X11, DESY-EMBL	Cu Kα	Cu Kα
space group	*P*1	*P*2	$P2_12_12_1$	*I*422
cell dimensions				
a, *b*, *c* (Å)	29.3, 54.2, 54.2	53.6, 99.3, 64.1	67.5, 103.7, 105.2	77.73, 77.73, 76.2
α, *β*, *γ* (deg)	α = 85.8, *β* = 74.31, *γ* = 74.3	*β* = 89.99	α = *β* = *γ* = 90	α = *β* = *γ* = 90
resolution range (Å)[a]	25.0−1.86 (1.93−1.86)	30.0−1.74 (1.8−1.74)	25−2.0 (2.07−2.0)	25.0−2.1 (2.18−2.1)
unit cell volume (Å^3)	79966	341400	736348	460460
mosaicity (deg)	0.59	0.66	0.8	0.75
observations	63129	265727	241674	65956
unique reflections	24461(2259)	69130 (6837)	49951 (4724)	6969 (617)
redundancy	2.6 (2.4)	3.8 (3.8)	4.8 (4.2)	9.5 (6.3)
completion (%)	94.1 (86.4)	99.8 (100)	98.7 (95.4)	98.2 (89.3)
$I/\sigma(I)$	28.85 (8.07)	14.85 (2.19)	16.9 (2.65)	20.3 (3.35)
R_{sym} (%)[b]	3.7 (10.5)	7.5 (53.6)	7.4 (36.5)	10 (45.7)
Molecules/A.U	4	8	8	1
pseudotranslation vector		0.5, 0.5, 0.5	0.0, 0.34, 0.5	
Refinement Statistics				
rmsd bonds (Å)	0.0051	0.0047	0.0054	0.0050
rmsd angles (deg)	1.09	1.17	1.11	1.08
R_{cryst} (%)[c]	17.2	19.2	20.6	22.1
R_{free} (%)	21.2	22.3	26.1	25.9
no. of residues	336	703	704	87
no. of atoms	3082	6307	6337	791
protein	2624	5348	5495	686
calcium	8	20	16	2
water	450	939	826	103
average *B*-factors (Å^2)				
protein (overall)	13.9	16.6	25.4	33.5
calcium	11.2	14.3	28.2	47.6
solvent atoms	26.5	29.1	34.8	46.7
Ramachandran plot, residues in				
most favored region	241 (87.3%)	552 (89%)	516 (85.9%)	67 (90%)
additionally allowed regions	33 (12%)	68 (11%)	82 (13.6%)	8 (10%)
generously allowed regions	2 (0.7)	1	3 (0.5%)	0

[a]Values in parentheses are for the highest resolution shell. [b]$R_{sym} = \sum|I(h) - \langle I(h)\rangle|/\sum I(h)$, where $I(h)$ is the observed intensity and $\langle I(h)\rangle$ is the mean intensity of reflection *h* over all measurements of $I(h)$. [c]R_{cryst} and $R_{free} = \sum_h||F(h)_o| - |F(h)_c||/\sum_h|F(h)_o|$. Throughout refinement, 5% of the total reflections were held aside for R_{free}.

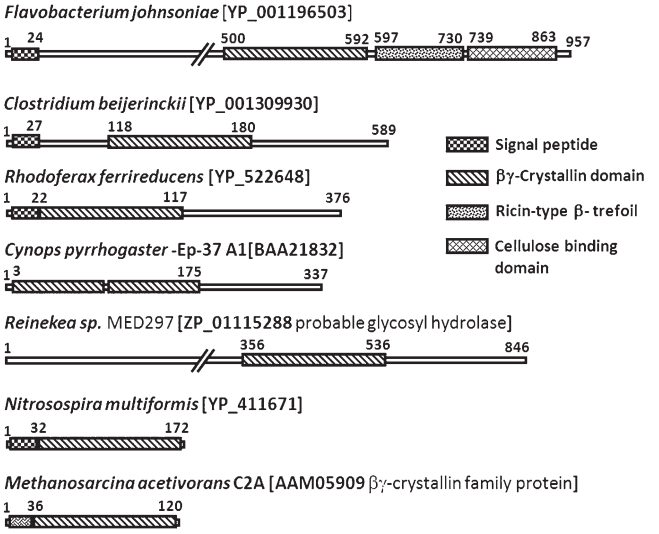

FIGURE 1: Schematic representation of the *βγ*-crystallin domain containing proteins from representative species from eukaryotes, archaea, and prokaryotes. Numbers in the domains represent residues between which the putative *βγ*-crystallin domain was identified. Domains from these proteins were used in this study.

R. ferrireducens (Gram −ve prokaryote), reinekllin from *Reinekea* sp. (Gram −ve prokaryote), nitrollin from *N. multiformis* (ammonia-oxidizing soil bacterium), and ep37 from *C. pyrrogaster* (amphibian-vertebrate). A list of these proteins with their sequence alignment with several other new members is shown in Figure 2. As seen in Figure 1, the *βγ*-crystallin domain in all of the proteins, except in nitrollin and M-crystallin, is a part of a bigger protein. In such cases, only the *βγ*-crystallin domain was selected for cloning and overexpression to avoid any ambiguity which may arise due to the role of the noncrystallin domain in Ca^{2+} binding. Such extensive recruitment as modules in proteins of varied functions clearly indicates that the domains of *βγ*-crystallin have universal roles in the functioning of proteins from multiple species.

βγ-Crystallin Domain Structure: Fold and Novelties. In order to explore the structural features and define the motif of Ca^{2+} binding in the proteins of the *βγ*-crystallin superfamily, we attempted to crystallize several proteins and were successful in crystallizing three proteins. In the process, three crystal structures of diverse domains (M-crystallin, clostrillin, and flavollin) were solved (Figure 3A−C, Table 1). They follow the conventional *βγ*-crystallin domain organization with two motifs, A and B,

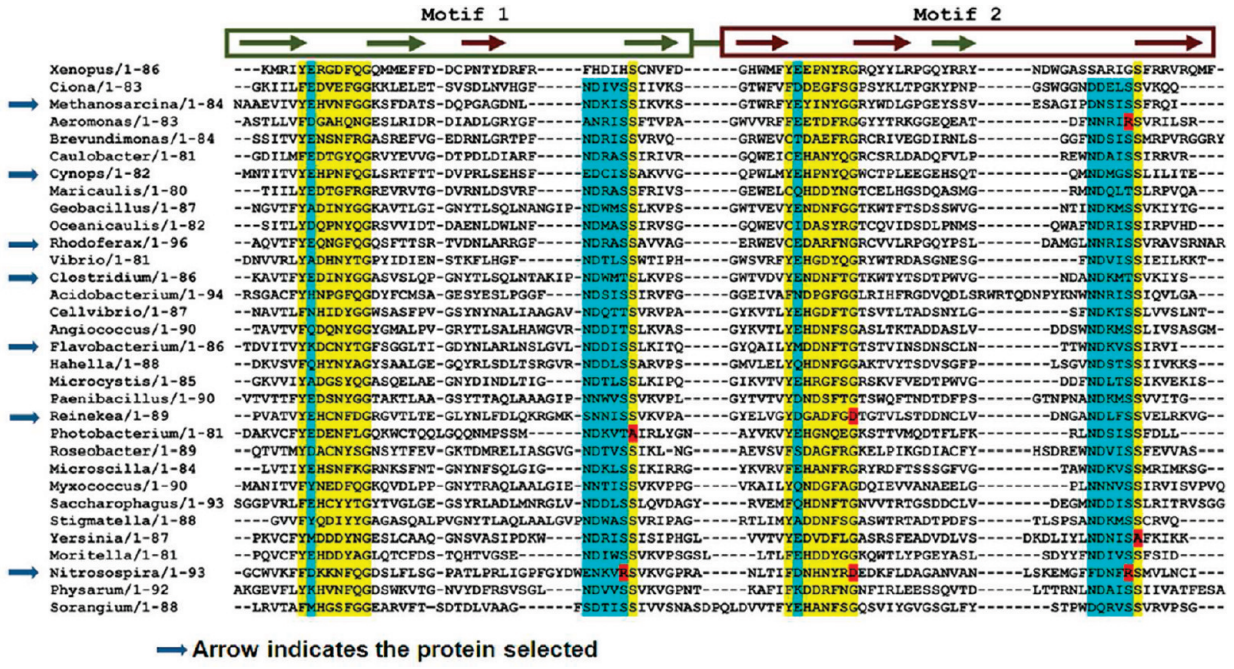

FIGURE 2: Multiple sequence alignment of novel $\beta\gamma$-crystallin domains (> 30 sequences) from various organisms. $\beta\gamma$-Crystallin signature regions are highlighted in yellow (Y/FXXXXFXG) and cyan (N/D-N/D-#-I-S/T). Only the $\beta\gamma$-crystallin region of the respective sequence was selected. Red highlighted residues indicate the natural replacements of largely conserved serine in a few isolated cases. The individual proteins (accession numbers) are *Xenopus* (NP_001072781, *Ciona* (PDB ID 2bv2), M-crystallin (AAM05909), *Aeromonas* (YP_857436), *Brevundimonas* (ZP_05032477), *Caulobacter* (NP_419840), *Cynops*-ep37 (BAA21832), *Maricaulis* (YP_757082), *Geobacillus* (ZP_03038350), *Oceanicaulis* (ZP_00952155), *Rhodoferax* (YP_522648), *Vibrio* (AAC12276), *Clostridium* (YP_001309930), *Acidobacterium* (YP_592325), *Cellvibrio* (YP_001980738), *Angiococcus* (CAF05655), *Flavobacterium* (YP_001196503), *Hahella* (YP_435570), *Microcystis* (YP_001655165), *Paenibacillus* (YP_003011846), *Reinekea* (ZP_01115288), *Photobacterium* (ZP_01220323), *Roseobacter* (YP_684280), *Microscilla* (ZP_01688128), *Myxococcus* (PDB ID 1NPS), *Saccharophagus* (YP_529394), *Stigmatella* (ZP_01467488), *Yersinia* (YP_001720039), *Moritella* (ZP_01896650), *Nitrosospira* (YP_411671), *Physarum* (P09353), and *Sorangium* (YP_001617452).

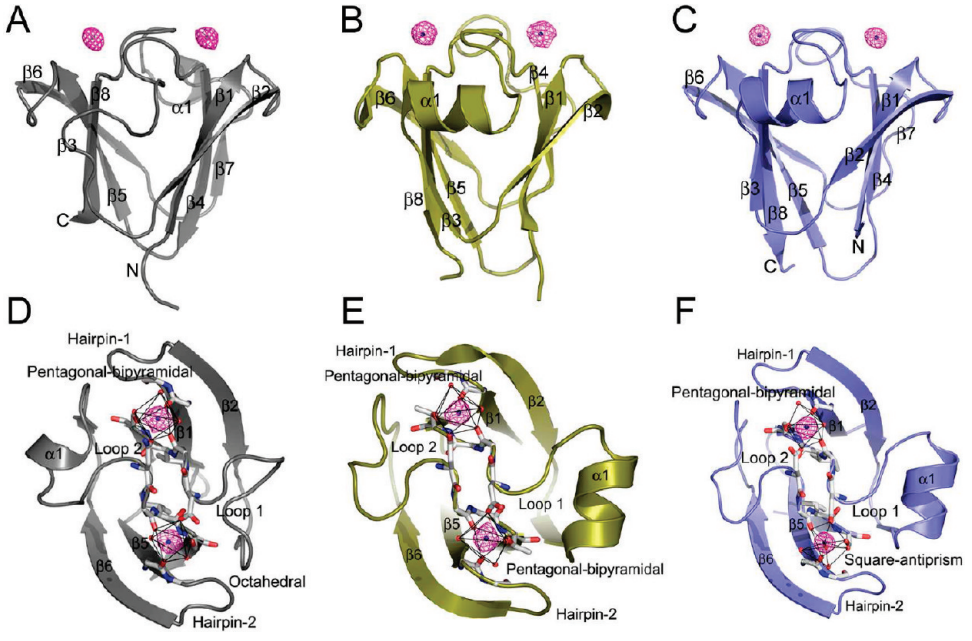

FIGURE 3: Ribbon diagrams of the three-dimensional structure of $\beta\gamma$-crystallin domains: (A) M-crystallin, (B) clostrillin, and (C) flavollin. Two bound Ca^{2+} per $\beta\gamma$-crystallin domain with $2F_o - F_c$ maps contoured at 2.0σ are shown. $\beta1$ to $\beta8$ represent the different β-strands of both Greek key motifs. Representation of Ca^{2+}-binding coordination geometries found in the three crystal structures of (D) M-crystallin, (E) clostrillin, and (F) flavollin.

comprising the wedge-like β-sandwich domains (Figure 3). The structure of M-crystallin exhibits an AB-type arrangement reminiscent of the vertebrate and urochordate members of the $\beta\gamma$-crystallin superfamily. The domain overlaps with the *Ciona* crystallin domain and γ-crystallin domains with an rmsd of 0.9 and 1.1 Å, respectively, for 80 Cα atoms. This structural homology is less when M-crystallin is compared to flavollin and clostrillin (rmsd of 1.6 Å for 75 Cα). These structural

differences are a result of the reversed arrangement of Greek key motifs found in prokaryotes (BA type) as compared to archaeal and vertebrate crystallins (AB type). Flavollin and clostrillin overlap with the protein S (1NPS) structure with an rmsd of 1.0 and 0.8 Å, respectively, for 86 Cα atoms.

The β-hairpin loops between strands 1 and 2 of each motif are characteristic signatures of $\beta\gamma$-crystallin domains. The first hairpin of flavollin presents a unique case in which, for the first time, a hairpin of the $\beta\gamma$-crystallin domain is found to be stabilized by the formation of a disulfide bridge. The bridge is formed between Cys9 and Cys70 of strand 7 and accentuates the H-bond formed between Ser40 (Ser34 equivalent of γ-crystallin) and the main chain carbonyl and amide of residues 8 and 11, respectively. The two sheets of the sandwich are connected by loops 1 (β3 to β4) and 2 (β7 to β8) on the roof of the domain. Strikingly, in all three structures, these loops form the Ca^{2+}-binding sites in the domains with a stoichiometry of 2 Ca^{2+} bound per domain.

Coordination Geometry. Each Ca^{2+}-binding site in a domain exhibits slightly altered coordination geometry. Assessments of coordination radii and geometry were done from multiple molecules found in the asymmetric units of different crystal forms (Table 1). In all three structures, Ca^{2+} is coordinated through pentagonal-bipyramidal geometry, with four oxygens from the protein chain and three from water at site 1. The average bonding distance at each of these sites varies in the range of 2.5−2.7 Å. Site 2 is more variable in terms of coordination in spite of the symmetry in the Ca^{2+}-binding sites. Coordination numbers at this site vary from 6, 7, or 8 with geometries of octahedral (M-crystallin), pentagonal-bipyramidal (clostrillin), and square-antiprismatic (flavollin), respectively, with similar calcium−oxygen bonding distances as in the case of site 1 (Figure 3D−F). Variability in Ca^{2+} coordination is contributed by water molecules whereas the protein chain contributes four oxygens at both of the sites in all three cases. In the three crystal structures, water molecules involved in calcium coordination ($-y$, $-z$) maintain a calcium−oxygen distance in the range of 2.65−3.0 Å. The main chain carbonyl oxygens ($+x$, $+y$) and the side chain oxygens ($+z$, $-x$) involved in coordination maintain a calcium−oxygen bond distance in the range of 2.45−2.8 Å.

Ca^{2+}-Binding Sites of $\beta\gamma$-Crystallin-like Proteins. Each Ca^{2+}-binding site has contributions from three components of the $\beta\gamma$-crystallin protein chain, the hairpin loop, loop 1 that forms the concavity of the site, and loop 2 which belongs to the second Greek key motif of the domain (Figure 4). In each site, the second residue of the hairpin loop, which is usually a polar amino acid, helps in direct ion coordination by employing its main chain carbonyl oxygen in the $+x$ position of the ion coordination sphere. The side chain of this residue plays an indirect role in ion binding by supporting a water molecule involved in ion coordination. The loops play a central role in Ca^{2+} binding due to the presence of an N/D-N/D-#-I-S/T-S motif (Figure 4) that forms the major part of the intercalated loops 1 and 2. The site 1 ion coordination is provided by the #-I-S/T of loop 1. The residue occupying the # position provides a main chain carbonyl for direct coordination of calcium at the $+y$ position (Figure 4A). This is followed by a residue (I) which is nonpolar in nature and contributes to the hydrophobic core of the domain, resulting in this region of the loop forming the base of the ion binding site. A serine or threonine following this residue coordinates calcium directly using its hydroxyl side chain. This arrangement is similar to that seen earlier in the case of protein S (*20*), spherulin 3a (*15*), and *Ciona* crystallin (*22*), thus suggesting that it is a well-designed

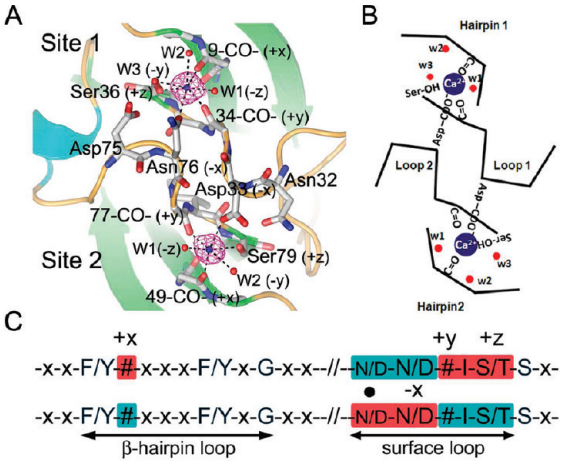

FIGURE 4: Representation of Ca^{2+}-binding sites: (A) M-crystallin seen with all of the species involved in calcium coordination. (B) Minimal site topology for calcium binding in a simplistic representation. (C) $\beta\gamma$-crystallin Ca^{2+}-binding motifs. Each Ca^{2+} is coordinated by residues of a single color (red/cyan). (-#-) represents residues coordinated by the main chain carbonyl. (-I-) represents hydrophobic residue, and (•) represents residue involved in indirect coordination through water.

ancestral motif of Ca^{2+} binding and it is widely spread in nature.

The ion coordinating serine is important as found in the case of protein S wherein a mutation of serine to arginine abrogated Ca^{2+} binding (*9*). This serine is at the $+z$ position in the coordination geometry and occurs ahead of the structurally important serine (equivalent to Ser34 of γ-crystallin) whose role is crucial in maintaining the conformation of the β-hairpin loop. Loop 2, which forms a part of the second Greek key motif, plays a role by acting *in trans*. The second Asn/Asp (equivalent to Asp33 or Asn76 in M-crystallin) residue of either of the loops provides monodentate coordination to Ca^{2+} and is coordinated by the opposite motif (Figure 4A). The first Asn/Asp (equivalent to Asn32, Asp75 in M-crystallin) residue plays an indirect role by coordinating the second water molecule that shares the $-y$ position with another water molecule (Figure 4A). This phenomenon of site formation by side chain coordination *in trans* between juxtaposed Ca^{2+}-binding sites can lead to simultaneous binding of Ca^{2+} to the two sites. The three regions are at mutually discrete locations in the primary sequence of the domain, which Ca^{2+} bridges together on binding. The internal symmetry among the two sites leads to an interlock formation like a "double clamp" that helps the discrete regions of the domains to come into contact on binding Ca^{2+} (Figure 4B). The organization of the site, therefore, requires the presence of an -N/D-N/D-#-I-S/T-S signature for ion binding at each individual motif (Figure 4C), which is independent of the AB-type or the BA-type arrangement of the Greek key motifs in the $\beta\gamma$-crystallin domains. The reversed arrangement of motifs is purported to be a result of a divergence at the single motif ancestor and subsequent evolution through gene duplication (*5*).

Interfacial Ca^{2+} Binding Site. In addition to the conventional sites found in all three proteins, the structure of flavollin exhibits a dimeric structure in the crystal lattice. The distinguishing feature of this dimeric arrangement is the presence of an interdomain Ca^{2+}-binding site mediating this dimeric association (Figure 5A). The dimeric interface comprises 440 $Å^2$, which is 9% of the total accessible surface area of the individual domain. The Ca^{2+}-binding site in this case is formed by the mutually

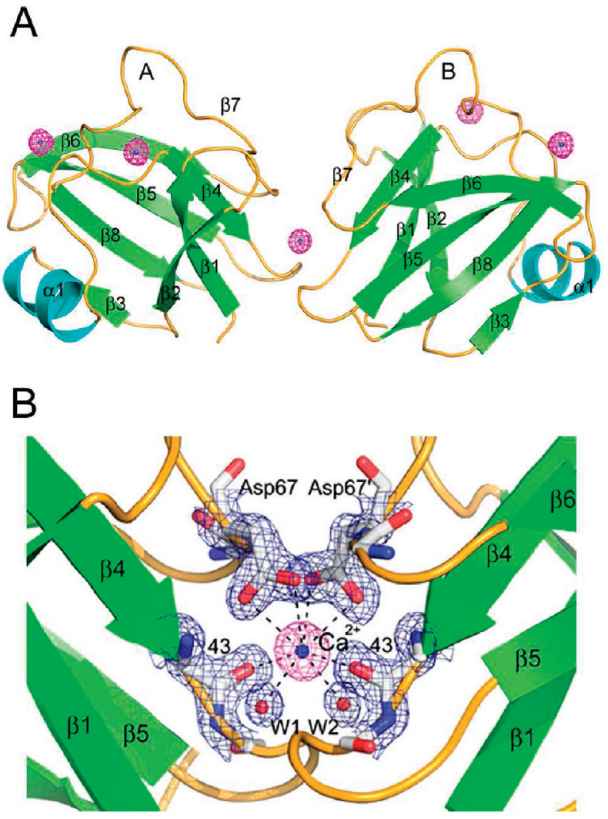

FIGURE 5: Representation of an unconventional interdomain Ca^{2+}-binding site found in the crystal structure of flavollin. (A) Arrangement of two $\beta\gamma$-crystallin domains with an interdomain Ca^{2+}-binding site; (B) mode of ligation with Asp67 from two domains. $2F_o - F_c$ maps of coordinating residues in blue were contoured at 1.2σ. Ca^{2+} $2F_o - F_c$ density was contoured at 2.0σ.

symmetric juxtaposition of the two linker loops between strands 4 and 5 and between strands 6 and 7 (Figure 5B).

Molecular Effects and Affinities toward Binding Ca^{2+}. The binding of Ca^{2+} to the various domains described is largely enthalpically driven as indicated by the negative sign in the binding isotherms. Clostrillin and ep37 show multiphasic Ca^{2+}-binding isotherms, which were fit using two sets of sites and sequential binding site models, respectively. The affinities shown by the $\beta\gamma$-crystallin domains are in the micromolar range, which is lower than the typical nanomolar range binding affinity exhibited by proteins of the EF-hand superfamily (Figure 6, Table 2). Overall dissociation constants for individual molecules vary from lower micromolar (4 μM for clostrillin) (Figure 6B) to higher micromolar (370 μM for rhodollin) (Figure 6D). Such wide-ranging affinities among different proteins are symbolic of altered responses of different domains to calcium. The binding of Ca^{2+} does not induce major structural reorganization in most $\beta\gamma$-crystallin members (data not shown). However, in order to dissect out the contributions from the various structural changes associated with the binding process, a comparison of the structures of the apo and Ca^{2+}-bound forms of the proteins would be required. Ca^{2+} binding evokes altered stabilization in these domains which manifests as an ~18 °C increase in melting temperature (T_M) in clostrillin and M-crystallin whereas in flavollin, T_M does not change upon binding Ca^{2+}. A case of moderate increase (~4 °C) in thermal stability is seen in the case of rhodollin, indicating once again the versatility of Ca^{2+}-binding responses in these domains (Figure 7). Earlier studies performed on individual $\beta\gamma$-crystallin domains from *Yersinia pestis* and *Caulobacter crescentus* (*Yersinia* crystallin and caulollins) revealed natively and partially unstructured domains in the apo form which attain structural elements upon binding calcium

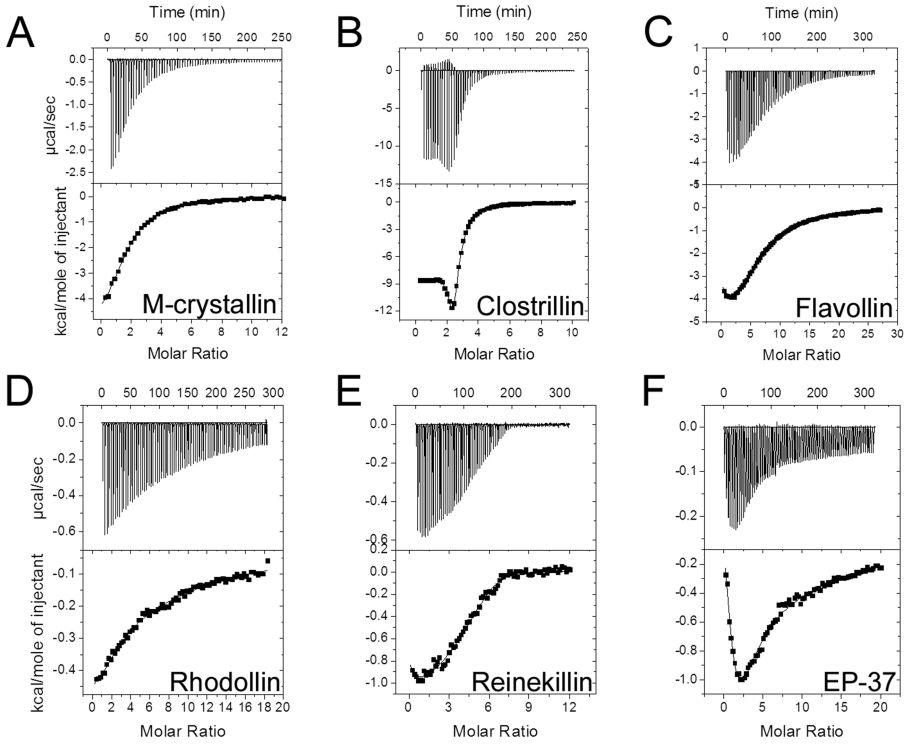

FIGURE 6: Isotherms of Ca^{2+} binding to various $\beta\gamma$-crystallin domains measured by ITC. Six different $\beta\gamma$-crystallin domains were selected: (A) M-crystallin, (B) clostrillin, (C) flavollin, (D) rhodollin, (E) reinkllin, and (F) ep37 A1. Appropriate protein concentrations (50−100 μM) were used in 50 mM Tris-HCl (pH 7.5) containing 50 mM KCl. In all titrations, 10 mM $CaCl_2$ prepared in the same buffer was loaded in the syringe. The data were best fitted to various models provided in the program. The best fit values of the macroscopic dissociation constant and ΔH are listed in Table 2.

Table 2: Thermodynamic Parameters of Ca^{2+} Binding to Various $\beta\gamma$-Crystallins by Isothermal Titration Calorimetry

proteins	model	K (mol^{-1})	K_d (μM)[a]	ΔH ($kcal \cdot mol^{-1}$)	ΔS ($cal \cdot mol^{-1} \cdot K^{-1}$)	ΔG ($kcal \cdot mol^{-1}$)
M-crystallin (archaeal)	sequential sites	$7.8 \times 10^4 \pm 1.2 \times 10^4$	32	−5.3	5.0	−6.8
		$1.2 \times 10^4 \pm 4.9 \times 10^2$		−5.2	1.3	−5.6
flavollin (prokaryote)	two set of sites	$1.1 \times 10^5 \pm 6.8 \times 10^4$	33	−2.1	16.0	−7.0
		$9 \times 10^3 \pm 421$		−6.3	−2.8	−5.4
clostrillin (prokaryote)	two set of sites	$3 \times 10^4 \pm 2.3 \times 10^3$	4	−43.4	−123	−6.1
		$2 \times 10^6 \pm 2.5 \times 10^5$		−8.5	0.77	−8.7
rhodollin (prokaryote)	two set of sites	$1.3 \times 10^4 \pm 9.8 \times 10^3$	370	−0.5	17.5	−5.8
		$5.5 \times 10^2 \pm 453$		1.9	6.3	−0.02
reinikillin (prokaryote)	sequential sites	$5.8 \times 10^3 \pm 1.2 \times 10^3$	40	−2.0	10.5	−5.2
		$1.1 \times 10^5 \pm 3 \times 10^4$		1.8	−141.5	44.7
ep37 (vertebrate)	sequential sites	$4.1 \times 10^4 \pm 3 \times 10^3$	260	−0.2	20.4	−6.4
		$2.9 \times 10^3 \pm 2.3 \times 10^2$		−10.2	−17.8	−4.8
		$2.1 \times 10^3 \pm 1.5 \times 10^2$		6.7	37.3	−4.6
		$0.9 \times 10^3 \pm 0.7 \times 10^2$		−14.9	−35.5	−4.1

[a] $K_d = 1/\sqrt{K_1 K_2}$ (K_d represents the overall dissociation constant).

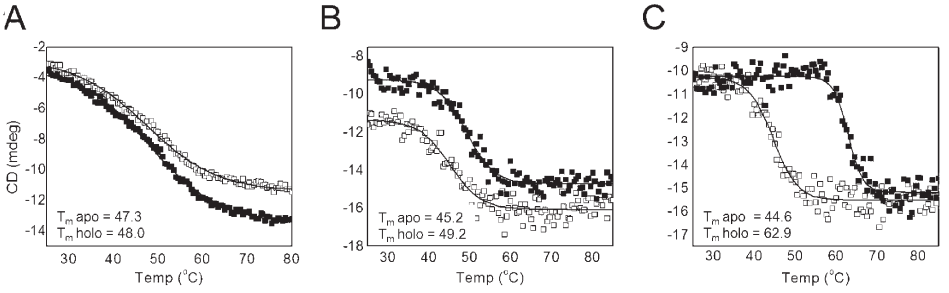

FIGURE 7: (A) Flavollin with almost insignificant change in T_m in the presence or absence of calcium. (B) Rhodollin with moderate increase (ΔT_m 4 °C) in thermal stability upon binding Ca^{2+}. (C) Clostrillin with significantly high increase in thermal stability (T_m increased by 18 °C) in the holoprotein. Proteins were used in the concentration range of 0.1−0.2 mg/mL with either 0.5 mM EDTA or 1 mM $CaCl_2$.

(*16*, *17*). Some of these $\beta\gamma$-crystallins, therefore, have the physicochemical potential to sense or sequester Ca^{2+} ions and possibly affect biochemical processes when recruited as modules in multidomain proteins.

Impaired Ca^{2+}-Binding Sites and Their Gain of Function. Many $\beta\gamma$-crystallin-like domains are not known to bind Ca^{2+}. In a recent study, a Ca^{2+}-binding disabled $\beta\gamma$-crystallin homologue, nitrollin, was reported by us (*27*). The loss of Ca^{2+} binding in this domain is attributed to the fact that the $+z$ position serines in both of the Greek key motifs have been replaced naturally by arginines (Arg88 and Arg133). Serine to arginine mutation is drastic as it alters polarity due to its positively charged guanidinium group and volume of the binding site due to a much longer side chain compared to serine (Figure 8A), which would result in loss of Ca^{2+} binding. In addition to mutations in serine residues, site 2 has a phenylalanine in place of Asn/Asp, which is involved in an indirect coordination by supporting a water molecule at the $-y$ position of the coordination sphere. Three mutations (R88S, R133S, and F129D) were introduced to provide the amino acids with the required side chains (R88S, R133S) and thus created an environment for indirect coordination of calcium through water using the F129D mutation. This mutant shows a recovery in its Ca^{2+}-binding properties when compared with wild type as analyzed using $^{45}Ca^{2+}$ overlay and fluorescence (Figure 8C,D). We could observe weaker binding to Ca^{2+} only with two mutations (R88S and R133S) in nitrollin, which is enhanced upon adding F129D. Due to precipitation, this gain-of-function mutant could not be concentrated enough to carry out ITC for measuring Ca^{2+} binding. Phe129 acts a nonpolar space-filling residue in the proximity of the hairpin 2 residues Asp102, Glu109, and Lys111 in the wild-type structure. An alteration in this residue to aspartate could lead to a disturbance in the local electrostatics of the region and subsequent loss in stability. In $\beta\gamma$-crystallin domains, alterations of some of the surface residues result in marked alterations in biophysical properties as seen in the case of γC-crystallin (*37*).

Interestingly, arginine or glycine is present at this position (in place of Ser, equivalent to Arg88 and Arg133 in nitrollin) in the Ca^{2+}-binding motifs of several proteins, including in lens β- and γ-crystallins, mainly from vertebrates (Figures 2 and 8B), leading to impaired Ca^{2+}-binding ability. In addition to arginine, there are other replacements and modifications in the N/D-N/D-#-I-S/T-S motif or in the vicinity. However, a detailed analysis is required to assess if these homologues would bind Ca^{2+} or not. It suggests that despite the presence of the fold, $\beta\gamma$-crystallins have naturally disabled variants which do not bind Ca^{2+}.

DISCUSSION

There are not many well-defined motifs for Ca^{2+} binding, except EF-hand motif and C2 domains (*38*, *39*). The EF-hand motif is a most widely studied helix−loop−helix motif where Ca^{2+} binds to a 12 amino acid loop region (*38*). C2 domains first identified in protein kinase C form another family of Ca^{2+} sensors of β-sandwich conformation (*39*). C2 domains bind two to three Ca^{2+} ions which are coordinated by the side chain and main chain oxygens in loop 1, loop 3, and loop 2 (*39*). In the Ca^{2+}-bound state, the C2 domains attain a capability to bind to membrane phospholipids. Besides the β-sandwich organization, the C2 domains bear no resemblance with the topology,

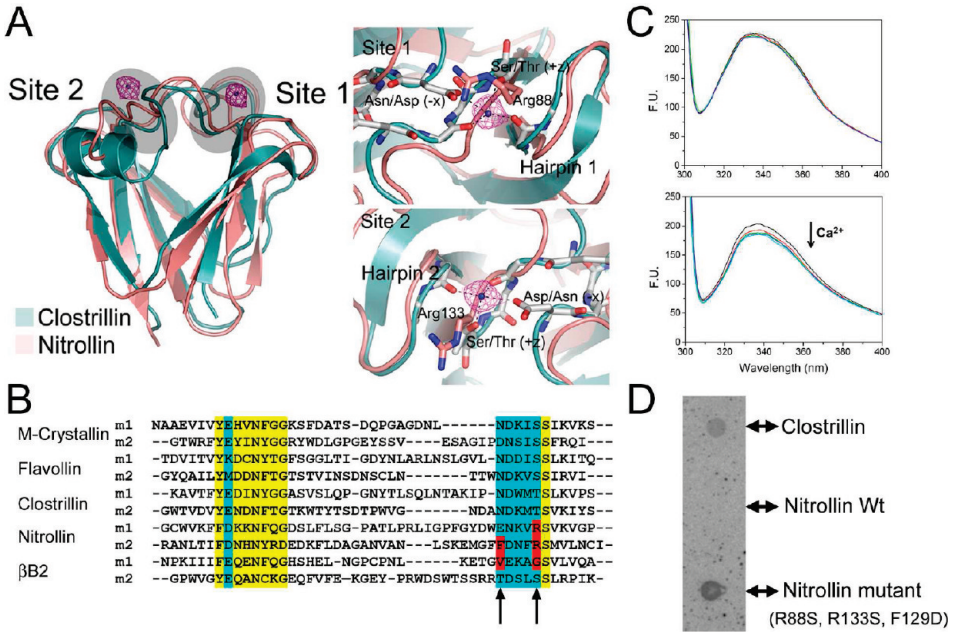

FIGURE 8: (A) Overlap of the nitrollin structure with clostrillin. Ca^{2+} density ($2F_o - F_c$) was contoured at 2.0σ. (B) Sequence alignment of four $\beta\gamma$-crystallins and lens βB2-crystallin. m1 and m2 represent motifs 1 and 2, respectively, in a domain. Nitrollin does not bind calcium due to natural mutation of Ser with Arg (depicted by arrows) and is selected as an example. The functional or prototype Ca^{2+}-binding motif of βB2-crystallin is shown. m1 and m2 represent the two motifs of individual domains. (C) Intrinsic Trp fluorescence titration of wild type (upper panel) and the nitrollin mutant (lower panel) with calcium. (D) Calcium-binding assay by ^{45}Ca by the membrane overlay method. Clostrillin was used as a positive control. As seen on the membrane, the nitrollin triple mutant shows bound calcium.

structural signatures, or the Ca^{2+}-binding motif of $\beta\gamma$-crystallins (*40*), making them a distinct set of Ca^{2+}-binding proteins.

The $\beta\gamma$-crystallin domains have varied affinities in the micromolar range (4−250 μM) as it is common for extracellular Ca^{2+}-binding proteins, whereas calcium sensors of the EF-hand family are generally high-affinity (lower micromolar to nanomolar range) Ca^{2+}-binding proteins. In some cases of $\beta\gamma$-crystallins, particularly vertebrate homologues (such as ep37) (*41*), the affinity for Ca^{2+} binding is much lower (Table 2). These proteins do not undergo major structural changes upon binding Ca^{2+} but have a reduced hydrodynamic size and generally attain high to moderate structural stabilization.

In human lens, calcium homeostasis is implicated in lens transparency and physiology, and a disturbance in ionic homeostasis is implicated in cataract (*42*). Though total Ca^{2+} concentration in a human lens is up to 100 μM, and more in the case of many cataractous lenses, only a few micromolar is in free form while the rest is in bound form (*42*−*44*). Though various mechanisms for Ca^{2+} signaling and homeostasis in the lens have been proposed (*43*, *45*), there are no known Ca^{2+}-binding proteins. One hypothesis could be that, in an eye lens, β- and γ-crystallins appropriately suit to this function owing to their low affinity for Ca^{2+} binding complemented by their abundant presence, although this is yet to be ascertained (*46*, *47*). Homologues of β- and γ-crystallins, such as protein S from *Myxococcus xanthus* and spherulin 3a from *P. polycephalum*, are found in some lower eukaryotic and prokaryotic species where they help the organism tide over periods of stressful environment in a Ca^{2+}-dependent manner (*10*, *13*). The crystal structures of three different homologues of $\beta\gamma$-crystallins along with the three structures (protein S, spherulin 3a, and *Ciona* $\beta\gamma$-crystallin) described earlier demonstrate the uniformity of the Ca^{2+}-binding site thereby forming a well-designed motif of Ca^{2+} binding prevalent in $\beta\gamma$-crystallins. This is further corroborated by studies on several other proteins (ep37 from cynops, an eukarya, rhodollin from *R. ferrireducens*, reinekllin from *Reinekea*) that have been shown to bind Ca^{2+} by ITC (Figure 6). All of these proteins have essential residues conserved at the N/D-N/D-#-I-S/T-S motif and thus would ligate Ca^{2+} similarly.

$\beta\gamma$-Crystallins, which are formed by an ancestral duplication event of a Greek key motif (*48*), have until recently been seen as structural components of vertebrate eye lens (*8*). The β- and γ-crystallins themselves have low but measurable affinity of Ca^{2+} binding owing to the modified sequence of the Ca^{2+}-binding sites in some Greek key motifs (*46*, *47*). However, one of the four Greek key motifs (second Greek key motif in βB2-crystallin) retains canonical residues (91-TDSLSS-96) capable of binding Ca^{2+}, which could be a reason for observing this binding (Figure 8B). In urochordate *Ciona intestinalis,* a $\beta\gamma$-crystallin protein is expressed in tissues (palps and otoliths) related to a primitive light sensing system (*22*). The crystal structure of this protein (PDB ID 2BV2) is very similar to lens $\beta\gamma$-crystallin domains, except for the presence of canonical N/D-N/D-#-I-S/T-S motif with bound Ca^{2+} (*22*). Urochordates do not have lenses, and thus *Ciona* $\beta\gamma$-crystallin could be considered as a close ancestor of vertebrate lens $\beta\gamma$-crystallins (*22*, *49*). The presence of this motif in archaeal homologues, as well as in *Ciona* crystallin, suggests that this Ca^{2+}-binding motif was present in ancestors, which was modified further during evolution to have no binding in many cases or weaker binding in lens $\beta\gamma$-crystallins.

Until recently, the superfamily predominantly consisted of vertebrate lens β- and γ-crystallins and their isoforms. Recent developments have yielded new insights into the $\beta\gamma$-crystallin members from nonlens tissues such as the cardiotoxic skin secretions of *Bombina maxima* and a highly complex six-domain-containing protein "absent in melanoma 1" (AIM1) (*50*, *51*). Genome sequences from multiple species are revealing new protein sequences in which $\beta\gamma$-crystallin-like domains with well-conserved Ca^{2+}-binding sites are found to be recruited as a part of multidomain proteins possibly to perform Ca^{2+}-dependent roles.

Interestingly, many $\beta\gamma$-crystallins, such as nitrollin, do not bind Ca^{2+}. In nitrollin, to prove the presence of a disabled motif, we were able to recreate Ca^{2+} binding, suggesting that the presence of Arg in place of Ser/Thr was one of the factors disabling the Ca^{2+} binding (Figure 8D). Based on the presence of Arg at the homologous position (in the place of Ser/Thr in N/D-N/D-#-I-S/T-S), we could identify many proteins with disabled Ca^{2+} binding. The number of proteins that does not bind Ca^{2+} is surprisingly much higher than generally seen in the case of other Ca^{2+}-binding motifs (such as the EF-hand), where only rarely a disabled motif is seen.

In conclusion, the $\beta\gamma$-crystallins are clearly versatile and dissimilar in terms of their Ca^{2+}-binding properties with well-known Ca^{2+}-binding motifs, such as EF-hand and C2 domains. They hence constitute a unique superfamily of Ca^{2+}-binding proteins with a well-designed motif. The unique aspect of this superfamily is the presence of nonfunctional motifs in a sizable number of proteins which indicate Ca^{2+}-independent functions of these domains. Biochemical roles of these domains in isolation and as modules in multidomain proteins, as seen in AIM1 (*51*), have to be worked out to understand the physiological consequences of Ca^{2+} binding. This is particularly relevant in prokaryote members as the presence of a large set of $\beta\gamma$-crystallin domain containing proteins would make it a prominent class of calcium-binding proteins. $\beta\gamma$-Crystallins along with a few EF-hand proteins and proteins with β-propeller structures are the only few classes of Ca^{2+}-binding proteins known so far in some bacteria, as roles for calcium in prokaryotic cell biology are a recently observed phenomenon (*52*−*54*). Through this work, we have explored the details and confirmed the widespread nature of the Ca^{2+}-binding motif in the $\beta\gamma$-crystallin superfamily, which was a role observed earlier but never convincingly established prior to this effort.

ACKNOWLEDGMENT

Critical comments on the manuscript by Dr. Graeme Wistow, NEI, NIH, and Dr. Christine Slingsby, Birkbeck College, are highly appreciated. We gratefully acknowledge the gifts of the genomic DNA of *Flavobacterium johnsoniae*, *Methanosarcina acetivorans*, *Reinekea* sp., and *Nitrosospira multiformis* from Dr. Mark J. McBride, University of Wisconsin, Professor William W. Metcalf, University of Illinois at Urbana−Champaign, Dr. Jarone Pinhassi, University of Kalmar, Sweden, and Dr. Lisa Stein, University of California, Riverside, respectively. The clone of ep37 was kindly provided by Dr. Kazuhito Takeshima, Nagoya University, Japan. We thank Dr. Santhosh Panjikar and the staff at EMBL, Hamburg, for help during data collection. We also thank Syed Sayeed Abdul for help in the laboratory.

REFERENCES

1. Clapham, D. E. (2007) Calcium signaling. *Cell 131*, 1047–1058.
2. Brown, E. M., Vassilev, P. M., and Hebert, S. C. (1995) Calcium ions as extracellular messengers. *Cell 83*, 679–682.
3. Wistow, G., and Piatigorsky, J. (1988) Lens crystallins: the evolution and expression of proteins for a highly specialized tissue. *Annu. Rev. Biochem. 57*, 479–504.
4. van Rens, G. L., de Jong, W. W., and Bloemendal, H. (1992) A superfamily in the mammalian eye lens: the beta/gamma-crystallins. *Mol. Biol. Rep. 16*, 1–10.
5. Jaenicke, R., and Slingsby, C. (2001) Lens crystallins and their microbial homologs: structure, stability, and function. *Crit. Rev. Biochem. Mol. Biol. 36*, 435–499.
6. Blundell, T., Lindley, P., Miller, L., Moss, D., Slingsby, C., Tickle, I., Turnell, B., and Wistow, G. (1981) The molecular structure and stability of the eye lens: x-ray analysis of gamma-crystallin II. *Nature 289*, 771–777.
7. Wistow, G., Turnell, B., Summers, L., Slingsby, C., Moss, D., Miller, L., Lindley, P., and Blundell, T. (1983) X-ray analysis of the eye lens protein gamma-II crystallin at 1.9 Å resolution. *J. Mol. Biol. 170*, 175–202.
8. Bloemendal, H., de Jong, W., Jaenicke, R., Lubsen, N. H., Slingsby, C., and Tardieu, A. (2004) Ageing and vision: structure, stability and function of lens crystallins. *Prog. Biophys. Mol. Biol. 86*, 407–485.
9. Teintze, M., Inouye, M., and Inouye, S. (1988) Characterization of calcium-binding sites in development-specific protein S of *Myxococcus xanthus* using site-specific mutagenesis. *J. Biol. Chem. 263*, 1199–1203.
10. Bagby, S., Harvey, T. S., Eagle, S. G., Inouye, S., and Ikura, M. (1994) Structural similarity of a developmentally regulated bacterial spore coat protein to beta gamma-crystallins of the vertebrate eye lens. *Proc. Natl. Acad. Sci. U.S.A. 91*, 4308–4312.
11. Sharma, Y., Rao, C. M., Narasu, M. L., Rao, S. C., Somasundaram, T., Gopalakrishna, A., and Balasubramanian, D. (1989) Binding site conformation dictates the color of the dye Stains-all: a study of the binding of this dye to the eye lens proteins crystallin. *J. Biol. Chem. 264*, 12794–12799.
12. Wistow, G. (1990) Evolution of a protein superfamily: relationships between vertebrate lens crystallins and microorganism dormancy proteins. *J. Mol. Evol. 30*, 140–145.
13. Rosinke, B., Renner, C., Mayr, E. M., Jaenicke, R., and Holak, T. A. (1997) Ca^{2+}-loaded spherulin 3a from *Physarum polycephalum* adopts the prototype gamma-crystallin fold in aqueous solution. *J. Mol. Biol. 271*, 645–655.
14. Kretschmar, M., Mayr, E. M., and Jaenicke, R. (1999) Homo-dimeric spherulin 3a: a single-domain member of the beta gamma-crystallin superfamily. *J. Biol. Chem. 380*, 89–94.
15. Clout, N. J., Kretschmar, M., Jaenicke, R., and Slingsby, C. (2001) Crystal structure of the calcium-loaded spherulin 3a dimer sheds light on the evolution of the eye lens betagamma-crystallin domain fold. *Structure 9*, 115–124.
16. Jobby, M. K., and Sharma, Y. (2005) Calcium-binding crystallins from *Yersinia pestis*: characterization of two single beta gamma-crystallin domains of a putative exported protein. *J. Biol. Chem. 280*, 1209–1216.
17. Jobby, M. K., and Sharma, Y. (2007) Caulollins from *Caulobacter crescentus*, a pair of partially unstructured proteins of $\beta\gamma$-crystallin superfamily gains structure upon binding calcium. *Biochemistry 46*, 12298–12307.
18. Barnwal, R. P., Jobby, M. K., Devi, M. K., Sharma, Y., and Chary, K. V. R. (2009) Solution structure and calcium-binding properties of M-crystallin, a primordial $\beta\gamma$-crystallin from archaea. *J. Mol. Biol. 386*, 675–689.
19. Giancola, C., Pizzo, E., Di Maro, A., Cubellis, M. V., and D'Alessio, G. (2005) Preparation and characterization of geodin. A betagamma-crystallin-type protein from a sponge. *FEBS J. 272*, 1023–1035.
20. Wenk, M., Baumgartner, R., Holak, T. A., Huber, R., Jaenicke, R., and Mayr, E. M. (1999) The domains of protein S from *Myxococcus xanthus*: structure, stability and interactions. *J. Mol. Biol. 286*, 1533–1545.
21. Wenk, M., and Jaenicke, R. (1999) Calorimetric analysis of the Ca(2+)-binding beta gamma-crystallin homolog protein S from *Myxococcus xanthus*: intrinsic stability and mutual stabilization of domains. *J. Mol. Biol. 293*, 117–124.
22. Shimeld, S. M., Purkiss, A. G., Dirks, R. P., Bateman, O. A., Slingsby, C., and Lubsen, N. H. (2005) Urochordate betagamma-crystallin and the evolutionary origin of the vertebrate eye lens. *Curr. Biol. 15*, 1684–1689.
23. Antuch, W., Guntert, P., and Wuthrich, K. (1996) Ancestral beta gamma-crystallin precursor structure in a yeast killer toxin. *Nat. Struct. Biol. 3*, 662–665.
24. Ohki, S. Y., Kariya, E., Hiraga, K., Wakamiya, A., Isobe, T., Oda, K., and Kainosho, M. (2001) NMR structure of *Streptomyces* killer toxin-like protein, SKLP: further evidence for the wide distribution of single-domain beta gamma-crystallin superfamily proteins. *J. Mol. Biol. 305*, 109–120.
25. Ohno, A., Tate, S., Seeram, S. S., Hiraga, K., Swindells, M. B., Oda, K., and Kainosho, M. (1998) NMR structure of the *Streptomyces* metalloproteinase inhibitor, SMPI, isolated from *Streptomyces nigrescens* TK-23: another example of an ancestral beta gamma-crystallin precursor structure. *J. Mol. Biol. 282*, 421–433.
26. Aravind, P., Wistow, G., Sharma, Y., and Sankaranarayanan, R. (2008) Exploring the limits of sequence and structure in a variant beta gamma-crystallin domain of the protein absent in melanoma-1 (AIM1). *J. Mol. Biol. 381*, 509–518.

27. Aravind, P., Suman, S. K., Mishra, A., Sharma, Y., and Sankaranarayanan, R. (2009) Three dimensional domain swapping in nitrollin, a single-domain beta gamma-crystallin from *Nitrosospira multiformis*, controls protein conformation and stability but not dimerization. *J. Mol. Biol. 385*, 163–177.
28. Rajini, B., Graham, C., Wistow, G., and Sharma, Y. (2003) Stability, homodimerization, and calcium-binding properties of a single, variant betagamma-crystallin domain of the protein absent in melanoma 1 (AIM1). *Biochemistry 42*, 4552–4559.
29. Otwinowski, Z., and Minor, W. (1997) Processing of X-ray diffraction data collected in oscillation mode. *Methods Enzymol. 276*, 307–326.
30. Collaborative Computational Project, Number 4 (1994) The CCP4 suite: programs for protein crystallography. *Acta Crystallogr., Sect. D 50*, 760–763.
31. Long, F., Vagin, A. A., Young, P., and Murshudov, G. N. (2008) BALBES: a molecular-replacement pipeline. *Acta Crystallogr., Sect. D: Biol. Crystallogr. 64*, 125–132.
32. Jones, T. A., Zou, J. Y., Cowan, S. W., and Kjeldgaard, M. (1991) Improved methods for building protein models in electron density maps and the location of errors in these models. *Acta Crystallogr., Sect. A: Found. Crystallogr. 47*, 110–119.
33. Brünger, A. T., Adams, P. D., Clore, G. M., DeLano, W. L., Gros, P., Grosse-Kunstleve, R., Jiang, J. S., Kuszewski, J., Nilges, M., Pannu, N. S., Read, R. J., Rice, L. M., Simonson, T., and Warren, G. L. (1998) Crystallography and NMR System: a new software suite for macromolecular structure determination. *Acta Crystallogr., Sect. D: Biol. Crystallogr. 54*, 905–921.
34. Laskowski, R. A., MacArthur, M. W., Moss, D. S., and Thornton, J. M. (1993) PROCHECK: a program to check the stereochemical quality of protein structures. *J. Appl. Crystallogr. 26*, 283–291.
35. Krissinel, E., and Henrick, K. (2007) Inference of macromolecular assemblies from crystalline state. *J. Mol. Biol. 372*, 774–797.
36. Holm, L., and Park, J. (2000) DaliLite workbench for protein structure comparison. *Bioinformatics 16*, 566–567.
37. Purkiss, A. G., Bateman, O. A., Wyatt, K., Wilmarth, P. A., David, L. L., Wistow, G. J., and Slingsby, C. (2007) Biophysical properties of gammaC-crystallin in human and mouse eye lens: the role of molecular dipoles. *J. Mol. Biol. 372*, 205–222.
38. McPhalen, C. A., Strynadka, N. C. J., and James, M. N. G. (1991) Calcium-binding sites in proteins: a structural perspective. *Adv. Protein Sci. 42*, 77–144.
39. Rizo, J., and Sudhof, T. C. (1998) C_2-domains, structure and function of a universal Ca^{2+}-binding domain. *J. Biol. Chem. 273*, 15879–15882.
40. Nalefski, E. A., and Falke, J. J. (1996) The C2 domain calcium-binding motif: structural and functional diversity. *Protein Sci. 5*, 2375–2390.
41. Ogawa, M., Takabatake, T., Takahashi, T. C., and Takeshima, K. (1997) Metamorphic change in EP37 expression: members of the $\beta\gamma$-crystallin superfamily in newt. *Dev. Genes Evol. 206*, 417–424.
42. Duncan, G., and Jacob, T. J. (1984) Calcium and the physiology of cataract. *CIBA Found. Symp. 106*, 132–152.
43. Duncan, G., Williams, M. R., and Riach, R. A. (1994) Calcium, cell signalling and cataract. *Prog. Retinal Eye Res. 13*, 623–652.
44. Tang, D., Borchman, D., Yappert, M. C., Vrensen, G. F., and Rasi, V. (2003) Influence of age, diabetes, and cataract on calcium, lipid-calcium, and protein-calcium relationships in human lenses. *Invest. Ophthalmol. Visual Sci. 44*, 2059–2066.
45. Rhodes, J. D., and Sanderson, J. (2009) The mechanisms of calcium homeostasis and signalling in the lens. *Exp. Eye Res. 88*, 226–234.
46. Rajini, B., Shridas, P., Sundari, C. S., Muralidhar, D., Chandani, S., Thomas, F., and Sharma, Y. (2001) Calcium binding properties of gamma-crystallin: calcium ion binds at the Greek key beta gamma-crystallin fold. *J. Biol. Chem. 276*, 38464–38471.
47. Jobby, M. K., and Sharma, Y. (2007) Calcium-binding to lens βB2- and βA3-crystallins suggests that all β-crystallins are calcium-binding proteins. *FEBS J. 274*, 4135–4147.
48. D'Alessio, G. (2002) The evolution of monomeric and oligomeric betagamma-type crystallins. Facts and hypotheses. *Eur. J. Biochem. 269*, 3122–3130.
49. Piatigorsky, J. (2006) Evolutionary genetics: seeing the light: the role of inherited developmental cascades in the origins of vertebrate lenses and their crystallins. *Heredity 96*, 275–277.
50. Qian, J. Q., Liu, S. B., He, Y. Y., Lee, W. H., and Zhang, Y. (2008) Beta gamma-CAT, a non-lens betagamma-crystallin and trefoil factor complex from amphibian skin secretions, caused endothelium-dependent myocardial depression in isolated rabbit hearts. *Toxicon 52*, 285–292.
51. Ray, M. E., Wistow, G., Su, Y. A., Meltzer, P. S., and Trent, J. M. (1997) AIM1, a novel non-lens member of the betagamma-crystallin superfamily, is associated with the control of tumorigenicity in human malignant melanoma. *Proc. Natl. Acad. Sci. U.S.A. 94*, 3229–3234.
52. Michiels, J., Chuanwu, X., Verhaert, J., and Vanderleyden, J. (2002) The functions of Ca^{2+} in bacteria: a role for EF-hand proteins? *Trends Microbiol. 10*, 87–93.
53. Tanaka, Y., Morikawa, K., Ohki, Y., Yao, M., Tsumoto, K., Watanabe, N., Ohta, T., and Tanaka, I. (2007) Structural and mutational analyses of Drp35 from *Staphylococcus aureus*: a possible mechanism for its lactonase activity. *J. Biol. Chem. 282*, 5770–5780.
54. Chen, C. N., Chin, K. H., Wang, A. H., and Chou, S. H. (2008) The first crystal structure of gluconolactonase important in the glucose secondary metabolic pathways. *J. Mol. Biol. 384*, 604–614.